



HAL
open science

Absolute sensitivity calibration of an extreme ultraviolet spectrometer for tokamak measurements

R Guirlet, JI Schwob, O Meyer, S Vartanian

► **To cite this version:**

R Guirlet, JI Schwob, O Meyer, S Vartanian. Absolute sensitivity calibration of an extreme ultraviolet spectrometer for tokamak measurements . 2016. hal-01369758

HAL Id: hal-01369758

<https://hal.science/hal-01369758>

Preprint submitted on 21 Sep 2016

HAL is a multi-disciplinary open access archive for the deposit and dissemination of scientific research documents, whether they are published or not. The documents may come from teaching and research institutions in France or abroad, or from public or private research centers.

L'archive ouverte pluridisciplinaire **HAL**, est destinée au dépôt et à la diffusion de documents scientifiques de niveau recherche, publiés ou non, émanant des établissements d'enseignement et de recherche français ou étrangers, des laboratoires publics ou privés.

Absolute sensitivity calibration of an extreme ultraviolet spectrometer for tokamak measurements

R. Guirlet^{a,1}, J.L. Schwob^b, O. Meyer^a, S. Vartanian^a

^aCEA, IRFM, F-13108 St-Paul-lez-Durance, France

^bRacah Institute of Physics, Hebrew University of Jerusalem, Israel

Abstract

An extreme ultraviolet spectrometer installed on the Tore Supra tokamak has been calibrated in absolute units of brightness in the range 10-340 Å. This has been performed by means of a combination of techniques. The range 10-113 Å was absolutely calibrated by using an ultrasoft-X ray source emitting six spectral lines in this range. The calibration transfer to the range 113-182 Å was performed using the spectral line intensity branching ratio method. The range 182-340 Å was calibrated thanks to radiative-collisional modelling of spectral line intensity ratios. The maximum sensitivity of the spectrometer was found to lie around 100 Å. Around this wavelength, the sensitivity is fairly flat in a 80 Å wide interval. The spatial variations of sensitivity along the detector assembly were also measured. The observed trend is related to the quantum efficiency decrease as the angle of the incoming photon trajectories becomes more grazing.

Keywords: extreme ultraviolet; spectroscopy; tokamaks; absolute calibration

1. Introduction

Extreme ultraviolet (EUV) spectroscopy is used extensively in various plasma physics research fields such as astrophysics and inertial and magnetic fusion. Its main interest resides in the detailed information it provides on the various species present in a plasma. It thus helps determine the qualitative composition of a plasma by the observation and identification of the spectral lines emitted by the ion species of the plasma. The density of the various emitting ions can also be deduced from spectroscopic measurements provided certain experimental conditions are fulfilled. One of them is that the spectral line intensities must be measured in absolute units. This necessitates that the spectroscopic instrument be calibrated in sensitivity.

¹ Corresponding author. Tel.: +33-442-25-38-85.
E-mail address: remy.guirlet@cea.fr

32 A commonly used method is the so-called line intensity branching ratio method [1, 2].
33 It consists of selecting spectral line pairs emitted by the same ion from one given upper level
34 to two different lower levels and comparing their measured intensity ratio with the theoretical
35 one. For this purpose, usually the spectrometer to be calibrated includes a visible line of sight
36 as close as possible to the EUV line of sight and connected to a visible spectrometer (for
37 which an absolute calibration is relatively easy). One line of the pair is chosen in the visible
38 range, and thus the sensitivity of the EUV spectrometer at the second line wavelength can be
39 deduced. This method has been used already many years ago on the TA 2000 torus [3, 4] and
40 is still in use nowadays, for example at JET for the SPRED VUV spectrometer in the range
41 130-360 Å [5]. Another way of calibrating an EUV spectrometer in absolute intensity units is
42 to compare the spectrometer signals with those of an already absolutely calibrated instrument,
43 as was done in [6] in the soft-X ray range.

44 In the present work, the Tore Supra tokamak is equipped with a high resolution, duo-
45 multichannel grazing incidence spectrometer [7] of the Schwob-Fraenkel type. Two
46 interferometrically aligned, ruled, concave gratings are mounted permanently on the
47 spectrometer. For most of the applications and in particular for the present measurements, a
48 600 g/mm grating blazed at 1.5° is used. It covers the 10-340 Å wavelength range. The
49 spectrometer is supported by a mobile structure which allows to spatially scan the lower half
50 of the plasma at a frequency 0.5 Hz.

51 Detection on this spectrometer is performed by means of two double microchannel
52 plate (MCP) detector assemblies in chevron configuration mounted on two carriages moved
53 independently along the materialised Rowland circle. The range of one detector is limited on
54 one end by the shortest wavelength mechanically accessible and on the other end by the
55 second detector assembly. It is thus called the 'short wavelength' (or SW) detector.
56 Conversely, the other assembly is limited by the SW detector and the longest wavelength
57 mechanically accessible, hence its name: 'long wavelength' (or LW) detector. The electrons
58 produced in the microchannels by impact of the incident EUV photons are converted into
59 visible photons by phosphor screens behind the MCPs and recorded by PDA (photodiode
60 array) cameras (one for either MCP assembly). An example of a spectrum recorded on the
61 LW detector is shown in Fig. 1.

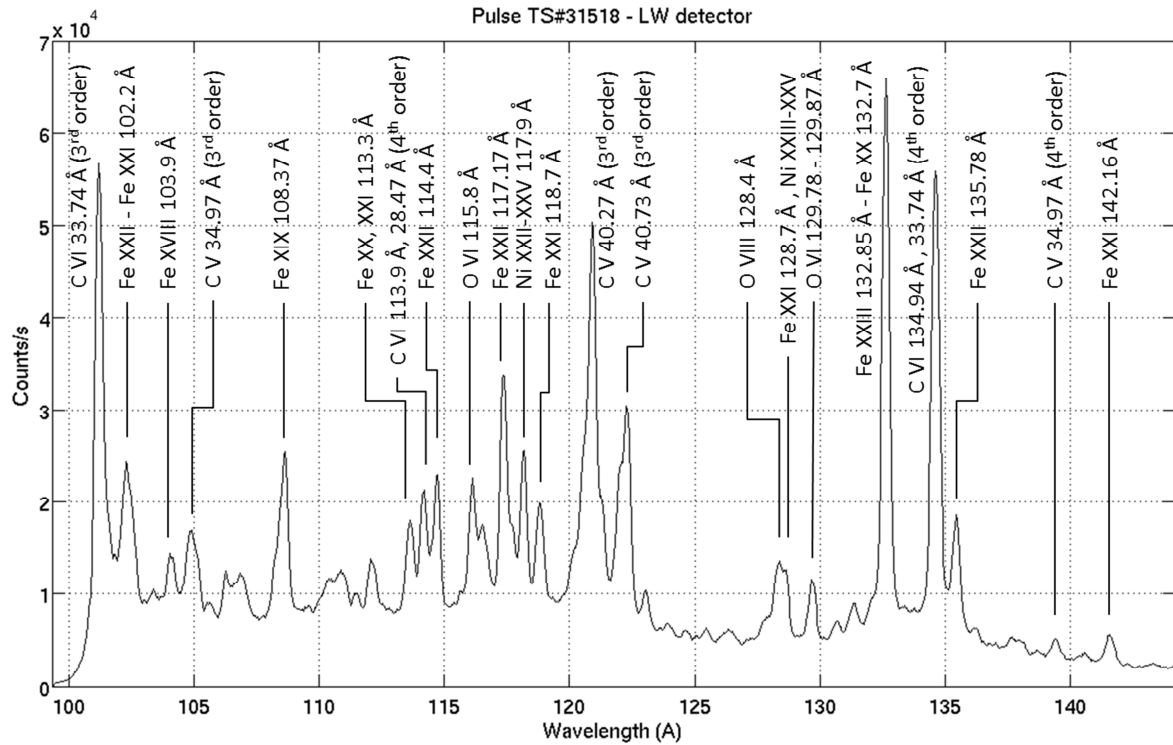
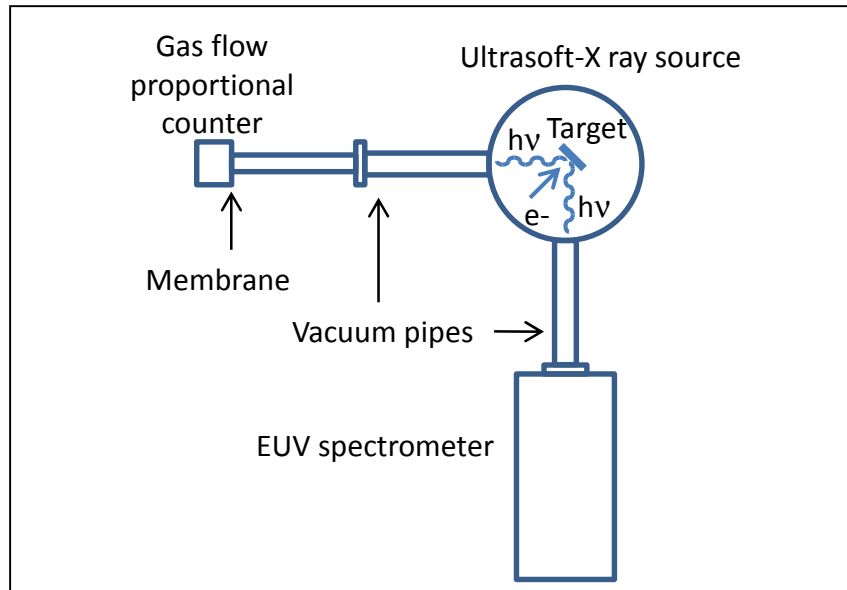


Figure 1: Spectrum recorded by the long wavelength detector with identification of the most prominent lines.

This spectrometer is not built with a visible line of sight so we could not use the branching ratio method exactly as presented in [1]. For the short wavelength part of the accessible domain we have used a combination of methods which are reported in this article. Section 2 describes the use of an ultrasoft-X ray source for absolute calibration in the 10-113 Å range. Section 3 describes the method used for calibration in the longer wavelength range, which combines the branching ratio method with a comparison of line intensity ratio measurements with collisional-radiative calculations, a method already used in [8]. Section 4 contains the results with a discussion on the uncertainties and a study of the spatial variation of the detector sensitivity. Section 5 presents a summary and conclusions.

2. Sensitivity calibration in the short wavelength range

2.1 Experimental setup and method



82
83
84

Figure 2: Absolute calibration setup with the ultrasoft-X ray Manson source

Target element	Wavelength (Å)
Mg	9.9
O	23.7
N	31.6
C	44.4
B	67.0
Be	113.0

85
86
87
88

Table 1: List of emitting elements in the various targets and wavelengths of the corresponding spectral lines.

89 In the short wavelength range, an absolute calibration was performed in the
90 spectroscopy laboratory with the help of a Manson Model 5 multi-anode ultrasoft-X ray
91 source [9]. The set-up is sketched on Fig. 2. The source emits photons at a given wavelength
92 (the so-called $K\alpha$ line) by electron beam impact on targets (playing the role of anodes for the
93 electrons) of various materials. A carousel of six targets allows to produce as many spectral
94 lines between 9.9 and 113 Å (see Table 1).

95 A gas flow proportional counter (GPC) is placed at 45° from the electron beam axis (a
96 setup very similar to the one used in [10]) to monitor the photon emission which can be as
97 high as 10^{12} photons/(s.sr). The GPC is set up so that it has a 100% efficiency. In order to
98 preserve its operating pressure, which is different from that in the source volume, a membrane

99 is placed in front of the counter as a separation from the source volume. The membrane
 100 transmission factor T_{GPC} depends on the wavelength, as shown in **Table 2**.

101

Wavelength (Å)	9.9	23.7	31.6	44.4	67.0	113.0
T_{GPC} (%)	55	42	32	19	50	37

102

103 **Table 2:** transmission factor of the membrane in front of the gas flow proportional counter

104

105 In addition, we have used a grid filter (transmission $T_F = 0.108$) to attenuate the GPC
 106 signal. The photon rate (in s^{-1}) measured by the GPC is thus given by:

$$107 \quad N_{GPC}^m(\lambda) = T_{GPC}(\lambda) \times T_F \times N_{GPC}^i(\lambda) \quad (1)$$

108

109 where $N_{GPC}^i(\lambda)$ and $N_{GPC}^m(\lambda)$ are the incident and measured photon rates respectively.

110 The spectrometer beam line is placed in a position symmetric to the GPC with respect
 111 to the electron beam to take advantage of the photon emission symmetry around the electron
 112 beam axis. The ratio of the photon rate incident on the spectrometer $N_{sp}^i(\lambda)$ to the photon rate
 113 $N_{GPC}^i(\lambda)$ incident on the GPC using a given target is equal to the solid angle ratio of the two
 114 detectors:

$$115 \quad \frac{N_{sp}^i(\lambda)}{N_{GPC}^i(\lambda)} = \frac{\Omega_{sp}}{\Omega_{GPC}} \quad (2)$$

116

117 Note here that $N_{sp}^i(\lambda)$ represents the total number of photons within the whole spectral line
 118 width excluding the background in the same spectral interval.

119 The spectrometer sensitivity at wavelength λ is defined as the ratio of the measured count rate
 120 to the incident photon rate:

$$121 \quad \eta(\lambda) = \frac{N_{sp}^m(\lambda)}{N_{sp}^i(\lambda)} \quad (3)$$

122 where $N_{sp}^m(\lambda)$ is the count rate measured by the spectrometer readout and acquisition system
 123 (expressed in counts/s in our setup). Due to the 100% efficiency of the gas counter and using
 124 **Eqs. 1** and **2**, one has:

$$125 \quad N_{sp}^i(\lambda) = \frac{\Omega_{sp}}{\Omega_{GPC}} N_{GPC}^i(\lambda) = \frac{\Omega_{sp}}{\Omega_{GPC}} \frac{N_{GPC}^m(\lambda)}{T_{GPC}(\lambda) T_F}$$

126 and thus:

127
$$\eta(\lambda) = \frac{N_{sp}^m(\lambda)}{N_{GPC}^m(\lambda)/(T_{CP}(\lambda)T_F)} \frac{\Omega_{GPC}}{\Omega_{sp}} \quad (4)$$

128

129 The spectrometer sensitivity can thus be deduced from the geometric parameters of the setup,
130 which are known, and the measurements of the detectors.

131

132 The tokamak plasma observed with the spectrometer is an extended light source. The
133 measurement performed by the spectrometer is thus the radiance (also commonly called
134 brightness) defined as:

135
$$B = (4\pi)^{-1} \times \int \varepsilon(l) dl \quad [\text{photons} / (\text{cm}^2 \text{ sr s})] \quad (5)$$

136

137 where ε (in $\text{cm}^{-3}\text{s}^{-1}$), called emissivity, is the photon rate emitted by plasma unit volume in a
138 given spectral line and l is the abscissa along the line of sight. The integral is performed over
139 the whole line of sight path within the plasma. The quantity we aim at determining is the
140 brightness calibration coefficient $K(\lambda)$ defined by:

141

142
$$B(\lambda) = K(\lambda) \times N_{sp}^m(\lambda) \quad (6)$$

143

144 over the whole wavelength range of the spectrometer. This quantity is crucial for plasma
145 applications since it is needed to relate the measured quantity $N_{sp}^m(\lambda)$ with the density of the
146 emitting ions. It can be obtained in the following manner. When a spectral line emitted in the
147 plasma is observed, the incident photon rate is by definition of $\eta(\lambda)$:

148
$$N_{sp}^i(\lambda) = \frac{N_{sp}^m(\lambda)}{\eta(\lambda)} \quad (7)$$

149

150 The spectral line brightness is thus given by:

151

152
$$B(\lambda) = \frac{N_{sp}^i(\lambda)}{(S\Omega)_{sp}} = \frac{N_{sp}^m(\lambda)}{\eta(\lambda) \times (S\Omega)_{sp}} \quad (8)$$

153

154 where $(S\Omega)_{sp}$ is the spectrometer geometric etendue (here S is the entrance slit area). The
155 brightness calibration coefficient is thus given by:

156

$$K(\lambda) = \frac{1}{\eta(\lambda) \times (S\Omega)_{sp}} \quad (9)$$

157

158 and is expressed in [photons/(s cm² sr)]/(counts/s).

159

160

161 **2.2 Results and comparison with a previous calibration**

162

163 The method exposed in the previous section has been applied to both the 'shorter wavelength'

164 (SW) and 'longer wavelength' (LW) detectors. The brightness calibration coefficient has been

165 determined for the six wavelengths available with the calibration source. It is shown in **Fig. 3**.

166 As the LW detector cannot be positioned to observe wavelengths shorter than 77 Å, only the

167 coefficient at 113 Å could be obtained by this method. Interestingly, it has almost the same

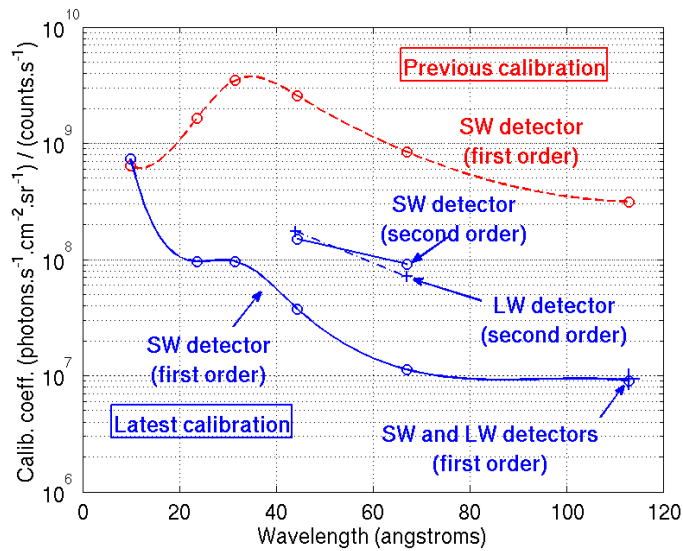
168 value as for the SW detector at the same wavelength. This observation results from the fact

169 that the two detectors are practically identical. It also denotes the accuracy of the

170 interferometric alignment of the spectrometer [7] and of the mechanical positioning of the

171 detectors along the Rowland circle to better than 25 µm. In the following we will thus not

172 distinguish between the two detectors on the calibration curves.



173

174 **Figure 3:** Absolute brightness calibration coefficient as a function of wavelength. SW

175 detector: (red ○ and dashed line) previous calibration in the first order and (blue ○ and

176 solid line) latest calibration in the first and second orders. LW detector: (blue + and dashed-

177 dotted line) latest calibration in the first two orders.

178

179 It can be seen from the slope of the calibration curve that on the short wavelength side
180 the spectrometer sensitivity (proportional to $1/K$) decreases with decreasing wavelength,
181 which illustrates the difficulty to measure spectral line intensities below 10 \AA with this
182 600g/mm gold coated ruled grating. The comparison of the latest calibration curve with the
183 previous one shows that the various improvements to the spectrometer (use of two
184 microchannel plates in chevron configuration for each detector assembly, installation of a new
185 grating, better performance PDA camera) have enhanced the spectrometer sensitivity by about
186 a factor 30 over the whole calibrated wavelength range except below about 20 \AA . The latter
187 feature is most likely due to the characteristics of the previous 600 l/mm holographic grating
188 which was platinum coated, while the new grating is a ruled one and gold coated with a
189 steeply decreasing efficiency toward the very short wavelengths below 15 \AA .

190

191 As this new grating is not designed to suppress the higher diffraction orders, the
192 ultrasoft X- ray source lines at 44.4 \AA and 67 \AA have also been observed in the second order
193 and have been used for the calibration, as shown in **Fig. 3**. They show that the spectrometer
194 sensitivity in the second order is poorer than in the first order, but only by a factor of 5 to 8.
195 We have actually observed intense spectral lines emitted by the tokamak plasma in as high an
196 order as the 7th or the 8th. Notice that the second order calibration is almost the same for the
197 SW and the LW detectors, another indication that the two detectors are practically identical.

198

199

200 **3. Sensitivity calibration in the long wavelength range**

201

202 **3.1 Use of the branching ratio method**

203

204 The mechanical design of the spectrometer presently equipped with two detector
205 carriages sets a lower limit of about 77 \AA to the spectral range accessible to the LW detector
206 (this limit is actually reached when the SW detector carriage is itself positioned at the shortest
207 possible wavelength position). The only line emitted by the ultrasoft X-ray calibration source
208 above this limit, and thus the only available one for the LW detector calibration in the first
209 order, is at 113 \AA . Therefore, another method has to be used in order to calibrate the
210 spectrometer up to its maximum wavelength, which reaches 340 \AA with the routinely used
211 600 g/mm grating.

212 The first additional method we use here is the so-called branching ratio method [1, 2],
 213 which we will now describe briefly. The emissivity ratio of two spectral lines of a given ion
 214 emitted by transitions from the same upper level to two different lower levels depends only on
 215 atomic constants and not on the plasma conditions. In tokamak plasmas the emission is
 216 completely dominated by spontaneous decay (rather than collisional de-excitation) so that the
 217 ratio can be written as:

218

$$219 \quad \frac{\varepsilon_{ij}}{\varepsilon_{ik}} = \frac{n_i A_{ij}}{n_i A_{ik}} = \frac{A_{ij}}{A_{ik}} \quad (10)$$

220

221 where n_i is the population density of the upper level i and A_{ij} and A_{ik} are the Einstein
 222 coefficients for spontaneous decay from levels i to levels j and k respectively. This relation
 223 holds as long as neither spectral line is self-absorbed by the plasma, i.e. when the plasma
 224 optical thickness can be neglected, which is the case here since the impurity ion density is
 225 always far below the main plasma ion density of about $5 \times 10^{19} \text{ m}^{-3}$. The effect of radiation
 226 trapping on the line brightness has been calculated using a mean transmission factor approach
 227 [2, 11] and the predictions were confirmed by measurements on the TA2000 torus [4]. It was
 228 found that for an optical thickness of the plasma below 0.1, the self-absorption is less than
 229 3.5%. It is thus negligible in the present experimental conditions.

230 Using Eq. (5) it is easy to show that the same relation can be used for the brightness
 231 ratio B_{ij}/B_{ik} measured by a spectrometer along a line of sight through the plasma. The relation
 232 between the measured signal ratio and the brightness ratio can be deduced from Eqs. 6 and
 233 10:

234

$$235 \quad \frac{K(\lambda_{ij}) N_{ij}^m}{K(\lambda_{ik}) N_{ik}^m} = \frac{B_{ij}}{B_{ik}} = \frac{A_{ij}}{A_{ik}} \quad (11)$$

236

237 This leads to the relation:

$$238 \quad \frac{K(\lambda_{ij})}{K(\lambda_{ik})} = \frac{N_{ik}^m A_{ij}}{N_{ij}^m A_{ik}} \quad (12)$$

239

240 This relation shows that the ratio of calibration coefficients at two different
 241 wavelengths can be deduced from line intensity measurements, which can be performed using

242 the tokamak plasma itself as a calibration source, and from Einstein coefficients, which are
 243 well known atomic constants in our case. This relation can thus be used for *relative*
 244 calibration for the two wavelengths λ_{ij} and λ_{ik} . This is particularly useful to determine the
 245 absolute calibration factor at either wavelength when it is already known at the other. As
 246 already said, the latter application is often used for VUV spectrometers using a visible
 247 spectrometer having the same line of sight [3,4,5].

248 As we did not have such a setup, we took advantage of the absolute calibration over
 249 the SW range described in the previous paragraph to calibrate the longer wavelength range by
 250 using spectral line pairs with one line below 113 Å (measured in absolute units with the SW
 251 detector) and the other at a wavelength to be calibrated above this value (measured with the
 252 LW detector). This procedure relies on the assumption that the two detectors have the same
 253 sensitivity at any given wavelength, an assumption supported by their identical design and by
 254 the identical absolute calibration coefficient found at 113 Å in Section 2.

255 In our case, the plasma emits few pairs of lines obeying the constraints imposed by the
 256 branching ratio method and the spectrometer wavelength coverage (two lines emitted from the
 257 same initial level of the same ion with a sufficient intensity, the wavelength of one between
 258 10 and 113 Å, the other between 113 and 340 Å). Only two suitable pairs were found, emitted
 259 by Carbon, the dominant impurity in Tore Supra plasmas. They are shown in **Table 3**. The
 260 calibration coefficients at 28.5 Å and 27.0 Å are calculated by a linear interpolation between
 261 the two closest calibration points obtained in Section 2, namely 23.7 Å and 31.6 Å.

262

LW spectral line			SW spectral line			Theoretical intensity ratio A_{ij}/A_{ik}
Transition	λ (Å)	A_{ij} (s^{-1})	Transition	λ (Å)	A_{ik} (s^{-1})	
n=3 \rightarrow n=2 (C VI)	182.2	5.72×10^{10}	n=3 \rightarrow n=1 (C VI Ly β)	28.5	7.23×10^{10}	0.79
n=4 \rightarrow n=2 (C VI)	134.9	1.09×10^{10}	n=4 \rightarrow n=1 (C VI Ly γ)	27.0	1.66×10^{10}	0.66

263

264 **Table 3:** Pairs of spectral lines and theoretical intensity ratios which have been used for
 265 relative calibration of the spectrometer above 113 Å.

266

267 This method provides invaluable information in that it allows to link the absolute
 268 calibration in the shorter wavelength range with the relative calibration in the longer

269 wavelength range. Nevertheless it is clearly not sufficient to calibrate the whole longer
 270 wavelength range of the spectrometer coverage. A complementary method is presented below.

271

272 3.2 Collisional-radiative modelling of line intensity ratios

273

274 The results of the branching ratio method exposed in the previous paragraph do not
 275 depend on the experimental conditions such as the plasma parameters and their time evolution
 276 or the spectrometer line of sight geometry. However, as it has just been shown, there are in
 277 general very few pairs of spectral lines which can be used in a given experimental situation.
 278 Relaxing the constraint of an identical upper level for the spectral line pairs used for the
 279 calibration, we find many groups of lines emitted by a given ion in the plasma within the
 280 relevant wavelength range. The drawback is that the relative intensities of the lines within a
 281 group depend not only on atomic physics but also on the plasma parameters. They can be
 282 calculated in the frame of a collisional-radiative model (CRM).

283 This calibration method, less accurate than the branching ratio method, has been
 284 applied on the SPRED VUV spectrometer at JET for the 360-980 Å range using spectral lines
 285 from mostly low ionisation stages [5]. In the present work, we aimed at calibrating a shorter
 286 wavelength range (130-340 Å) than at JET. We also wanted to avoid using spectral lines
 287 emitted near the plasma edge, where the plasma parameters are not so well known (in
 288 particular the electron temperature). For both these reasons we did not select very low
 289 ionisation stages, as can be seen on **Table 4**.

290

Emitter	Wavelength (Å)	Transition
C IV	222.8	$1s^2 2s^2 S - 1s^2 5p^2 P^o$
	244.9	$1s^2 2s^2 S - 1s^2 4p^2 P^o$
	259.5	$1s^2 2p^2 P^o - 1s^2 5d^2 D$
	262.6	$1s^2 2p^2 P^o - 1s^2 5s^2 S$
	289.2	$1s^2 2p^2 P^o - 1s^2 4d^2 D$
	296.9	$1s^2 2p^2 P^o - 1s^2 4s^2 S$
	312.4	$1s^2 2s^2 S - 1s^2 3p^2 P^o$
C VI	27.0	1 – 4 (Ly γ)
	28.5	1 – 3 (Ly β)

	134.9 + 135.0	2 – 4 (Balmer β)
	182.1 + 182.2	2 – 3 (Balmer α)
O V	151.5	2s2p $^3P^o$ - 2s4d 3D
	192.8 + 192.9	2s2p $^3P^o$ - 2s3d 3D
O VI	129.8 + 129.9	1s ² 2p $^2P^o$ - 1s ² 4d 2D
	150.1	1s ² 2s 2S - 1s ² 3p $^2P^o$
	172.9 + 173.1	1s ² 2p $^2P^o$ - 1s ² 3d 2D
	183.9 + 184.1	1s ² 2p $^2P^o$ - 1s ² 3s 2S
Fe XXIV	192.0	1s ² 2s 2S - 1s ² 2p $^2P^o_{3/2}$
	255.1	1s ² 2s 2S - 1s ² 2p $^2P^o_{1/2}$

291

292 **Table 4:** *Spectral lines used in the branching ratio method for absolute calibration transfer*
 293 *(in bold) and in the CRM line ratio method for relative calibration.*

294

295 In the collisional-radiative modelling, instead of expressing the line emissivity as a
 296 function of the population density of the initial level of the transition (as in **Eq. 10**), we use
 297 the total density n_z of the emitting ion. The emissivity of a given line between levels i and j
 298 can be written as:

299

$$300 \quad \varepsilon_{ij} = n_e n_z PEC_{ij}(n_e, T_e), \quad (13)$$

301

302 where n_e and T_e are the electron density and temperature respectively. The PEC_{ij} quantity,
 303 called photon emission coefficient, is calculated with a collisional-radiative model (CRM). It
 304 depends in a complex way on the collisional and radiative atomic processes in the plasma,
 305 namely transitions between excited levels of the emitting ions, recombination onto and
 306 ionisation from excited levels. The PEC dependence on n_e is generally weak and will be
 307 neglected here. In the present case the PEC values were obtained from the ADAS data and
 308 model **[12]**.

309 From **Eq. 13** it can be deduced that the emissivity ratio of two lines ij and kl emitted
 310 by the same ion is equal to the PEC ratio. For the brightness, which is the quantity actually
 311 measured by the spectrometer, the situation is slightly more complex:

$$312 \frac{B_{ij}}{B_{kl}} = \frac{\int n_e n_z PEC_{ij}(T_e) dl}{\int n_e n_z PEC_{kl}(T_e) dl} \quad (14)$$

314 where the integration is done along the line of sight. The exact calculation requires that we
 315 know the spatial distribution of all quantities in the integrals, in particular the emitting ion
 316 density profile along the line of sight. The most accurate way to obtain this is from a
 317 dedicated transport study [13], a sophisticated and somewhat lengthy procedure. Instead, we
 318 make here the rougher assumption that the PECs do not depend on T_e . This is verified in our
 319 case because the emitting layer of the selected ions in this study is very narrow. As an
 320 additional precaution, we have rejected lines with PECs depending strongly on the
 321 temperature in the T_e range where the emitting ion is abundant (e.g. C V 40.3 Å, $1s^2 \ ^1S_0 -$
 322 $1s2p \ ^1P_1^o$). As a consequence, denoting T_e^{em} the electron temperature of the emitting layer, the
 323 measured brightness ratio will thus be approximately equal to the PEC ratio:

$$324 \frac{B_{ij}}{B_{kl}} = \frac{PEC_{ij}(T_e^{em})}{PEC_{kl}(T_e^{em})} \quad (15)$$

325 An accurate determination of T_e^{em} would require either a full transport study, as
 326 already mentioned, or enough lines of sight to determine experimentally the position of the
 327 emission layer. The weak T_e dependence requested from the PECs retained in this study
 328 allowed to estimate T_e^{em} without loss of accuracy from the position of the emitting layers as
 329 calculated by a local ionisation balance calculation.

330 Denoting again N_{ij}^m the measured signal and $K(\lambda_{ij})$ the corresponding calibration
 331 coefficient, one gets by definition of the calibration coefficient (**Eq. 6**):

$$332 \frac{B_{ij}}{B_{kl}} = \frac{K(\lambda_{ij}) N_{ij}^m}{K(\lambda_{kl}) N_{kl}^m} \quad (16)$$

337

338 Provided the calibration coefficient is known at one wavelength, say λ_{ij} , the coefficient at the
 339 other wavelength λ_{kl} can be obtained by using **Eq. 15**:

340

$$341 \quad K(\lambda_{kl}) = K(\lambda_{ij}) \frac{N_{ij}^m}{N_{kl}^m} \frac{PEC_{kl}}{PEC_{ij}} \quad (17)$$

342

343 Comparing the calculated and measured C VI line brightness ratios, we have
 344 calculated the absolute calibration coefficients at 134.9 Å and 182.2 Å. Note that at 134.9 Å
 345 the Balmer β line is blended with the fourth order of the C VI Ly α line at 33.7 Å. In order to
 346 subtract the latter contribution it was necessary to estimate the grating efficiency in the fourth
 347 order. This was done by measuring the intensity of the well resolved C V 34.97 Å line in the
 348 first and fourth orders in identical pulses designed for the calibration described here (see next
 349 Section). This allowed us to deduce that the grating efficiency in the fourth order with respect
 350 to that in the first order is about 10% at this wavelength. The contribution of the fourth order
 351 C VI Ly α line to the measured 134.9 Å intensity was then calculated using the measured first
 352 order C VI Ly α line intensity and the fourth order efficiency. It was then subtracted from the
 353 measured intensity at 134.9 Å before the calibration coefficients were calculated.

354 Then we interpolate the calibration coefficient of the 150.1 Å line of the O VI group
 355 between the values at 134.9 Å and 182.2 Å. From there, we use **Eq. 17** with the O VI line
 356 group to obtain the calibration coefficients at 129.9 Å, 173 Å and 184 Å. Then with the same
 357 hypothesis we obtain the 151.5 Å (O V group) calibration coefficient, and this allows us to
 358 obtain the calibration coefficient at the second wavelength of the O V group, 192.9 Å. With
 359 the same reasoning, we obtain the calibration coefficients at 192.0 Å and 255.1 Å (Fe XXIV
 360 group) and at the six wavelengths of the C IV group. It has been checked that the final result
 361 (the curve which will be fitted to the data points) remains within the error bars if the order in
 362 which the line groups are added is changed.

363

364 **4. Results and uncertainties**

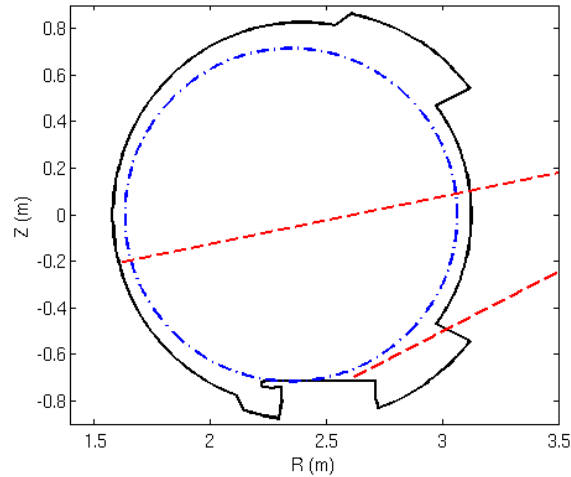
365

366 **4.1. Results**

367

368 A series of identical, ohmic pulses have been performed to record the useful spectral
 369 line brightnesses (Tore Supra pulses TS#31512 to TS#31519). The plasmas are found to be

370 very stationary and reproducible so there was no need to perform a multi-pulse statistical
371 study of the line ratios. The spectrometer was used in its spatial scanning mode, which means
372 that the whole spectrometer was rotated around a horizontal axis located in front of the
373 apparatus. In this mode of operation, the lower half of the plasma (see **Fig. 4**) could be
374 scanned at a period of 0.5 Hz.



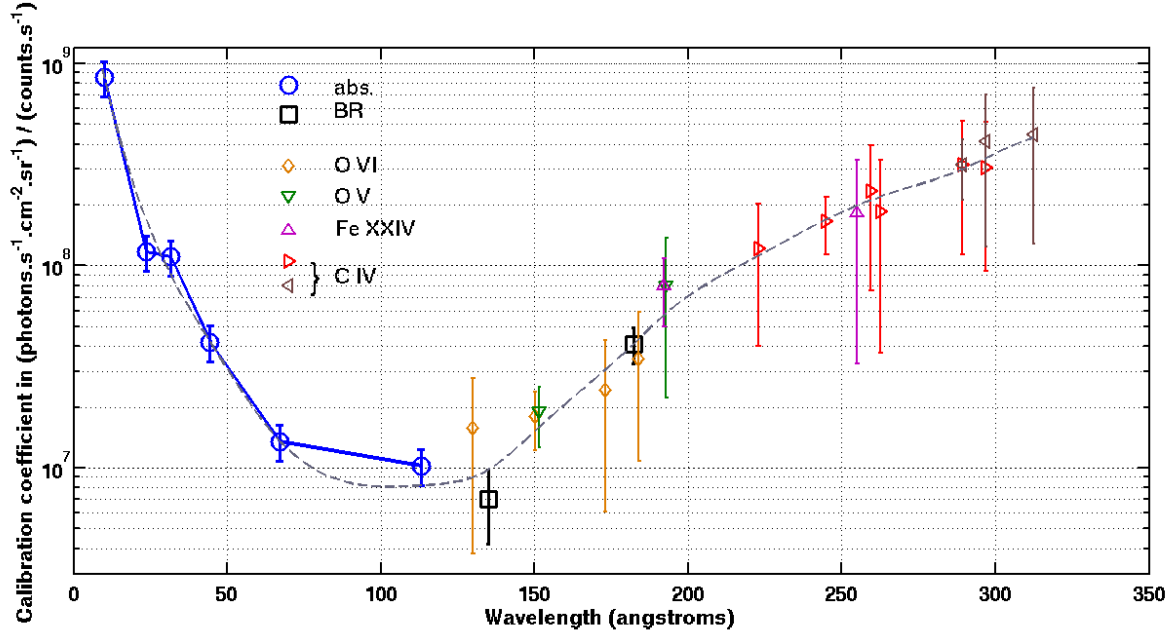
375
376
377
378
379

Figure 4: *Poloidal cross section (solid line) of the tokamak vessel, (dashed-dotted line) of the plasma last closed flux surface and (dashed line) of the extreme positions of the line of sight.*

380 Both the spectral line shapes and the radial profiles were used to reject blended lines.
381 In the case of the Fe XXIV lines, observed to be blended in [5], the analysis of the radial
382 brightness profiles allows to distinguish them from blended light species lines.

383 The calibration coefficients obtained with this method have been added to the results
384 obtained in Section 2.2. The overall calibration curve is shown in **Fig. 5**. It shows a broad
385 minimum (corresponding to a maximum in sensitivity) around 100 Å over a range of about 70
386 Å. The spectrometer sensitivity decreases steeply on both sides, although in the long
387 wavelength direction the slope tends to become lower. This indicates that with the same
388 grating a modified spectrometer with a longer mechanical range for the detector would be
389 sensitive enough to provide information over a broader wavelength range. This has been done
390 for the Schwob-Fraenkel spectrometer installed on the Berlin EBIT experiment [14, 15]. On
391 the contrary, in the short wavelength direction the slope is steeper and steeper. This indicates
392 that extending the mechanical range to shorter wavelengths would not provide additional
393 useful information below 10 Å.

394



395
 396 **Figure 5:** Absolute brightness calibration in lab (solid line with \circ), calibration transfer using
 397 the branching ratio method (\square) and relative calibration using the CRM of line ratios with
 398 plasma (the symbols are explained on the figure). The grey dashed line is a spline among the
 399 points and is adopted as the final calibration curve.

401 4.2. Uncertainties

402
 403 In the wavelength range absolutely calibrated with the ultrasoft-X ray source (9.9 -
 404 113 Å), the main uncertainty is that associated with the spectral line intensities measured with
 405 the spectrometer. It is mostly due to the uncertainty on the background estimate, which can be
 406 difficult for the weaker lines of the calibration source. The uncertainty on these intensities is
 407 at maximum 10% (it can be as low as 5% for the stronger lines). In addition, we estimate an
 408 uncertainty of 10% to take account of the geometric aperture uncertainty. The uncertainty on
 409 the proportional gas counter measurements is negligible compared to those associated with
 410 the spectrometer measurements. We have thus a global uncertainty of 20% for the calibration
 411 coefficients up to 113 Å.

412 For the calibration points using the branching ratio method, we must take into account
 413 the time fluctuations of the two spectral line intensities used for each point. These fluctuations
 414 are not negligible even during the stationary phase of the plasma. They are actually much
 415 larger than the statistical error (which is the square root of the time average signal if a Poisson
 416 distribution is assumed). The total uncertainty is thus estimated to 40% at 134.9 Å and 32% at
 417 182.2 Å.

418 For the CRM calibration method, a part of the uncertainty associated with the
 419 reference line (at wavelength λ_0) of a given line group is determined from the time fluctuation
 420 of the measured signal as discussed in the previous paragraph. To this fluctuation uncertainty,
 421 an uncertainty of 30% is added, corresponding to the interpolation of this reference line
 422 between two already calibrated wavelengths. For any other line (wavelength λ) of the group,
 423 the uncertainty is deduced from **Eq. 17**:

424

$$425 \quad \frac{\Delta K(\lambda)}{K(\lambda)} = \frac{\Delta K(\lambda_0)}{K(\lambda_0)} + \frac{\Delta \left(\frac{PEC(\lambda)}{PEC(\lambda_0)} \right)}{\frac{PEC(\lambda)}{PEC(\lambda_0)}} + \frac{\Delta N^m(\lambda)}{N^m(\lambda)} + \frac{\Delta N^m(\lambda_0)}{N^m(\lambda_0)} \quad (18)$$

426

427 The relative uncertainties on the signals $N^m(\lambda)$ and $N^m(\lambda_0)$ are calculated from the time
 428 fluctuations of the measurements, as said above. The uncertainty on the PECs themselves is
 429 difficult to assess and not always available in the literature. It seems that a global value of
 430 30% for all PEC ratios reflects satisfactorily both the accuracy of the atomic physics
 431 calculations and the residual PEC ratio dependence on T_e^{em} (see above the discussion about
 432 **Eq. 15**).

433

434 For a practical purpose, a curve has been fitted on the points in **Fig. 5**. The most
 435 satisfactory result was obtained with a spline. Below 120 Å the 20% uncertainty estimated for
 436 the absolute calibration points can be retained. Between 120 and 180 Å, where line intensity
 437 branching ratios were available, an uncertainty of about 35% is estimated. Above this
 438 wavelength, a value of 50% reflects satisfactorily the spreading and uncertainties of the
 439 relative calibration points. In this range, the uncertainty might be an underestimate of the
 440 actual uncertainty due to the use of the CRM, for which the uncertainties are not well known.

441

442

443

444 **5. Spatial variations of the detector response**

445

446 The tolerances of the spectrometer design and realisation are very tight, so that most
 447 mechanical pieces are positioned to less than 25 µm. Nevertheless, the response of the
 448 detector assembly along its length (i. e. along the wavelength direction) is not perfectly

449 uniform. It can be due to several reasons such as the small inhomogeneities of the
 450 multichannel plate and phosphor screen responses, the transmission of the fiber optics bundle
 451 or the quantum efficiency dependence on the photon incidence angle on the MCP input face.

452 As the non-uniformity and the spatial variation of the detector response play a role in
 453 the estimate of the spectral line absolute brightnesses, it has been measured for the LW
 454 assembly. The simplest way of doing this measurement is to select a spectral range containing
 455 well isolated spectral lines and perform several measurements, moving the detector by small
 456 position shifts between measurements in such a way that the spectral lines would strike
 457 different parts of the MCP.

458 Due to programme constraints, this method could not be applied in the spectroscopy
 459 laboratory. Therefore we have used the same series of identical discharges on the Tore Supra
 460 tokamak as for the calibration. During this series, the detectors were moved in a limited
 461 number of positions. As a result of this procedure, many spectral lines could be measured at a
 462 few positions on the detector. By comparing the spectrometer measurements of a given
 463 spectral line in the various positions and synthetising the results for all lines, we were able to
 464 deduce the non-uniformity and spatial variation of the detector assembly response. The list of
 465 the lines used for this procedure is given in **Table 5**.

466

Wavelength (Å)	Emitter
129.9	O VI
132.9	Fe XXIII
134.9	C VI 2-4 (+ Ly α 4 th order)
135.8	Fe XXII
238.5	O IV, C IV
241.5	C V (40.3 Å 6 th order)
244.9	C IV
281.9	C V
284.1	Fe XV
289.2	C IV
292.0, 291.3	Ni XVIII, C III

467

468 **Table 5:** *List of spectral lines and corresponding emitters for the evaluation of the non-*
 469 *uniformity and spatial variation of the detector response.*

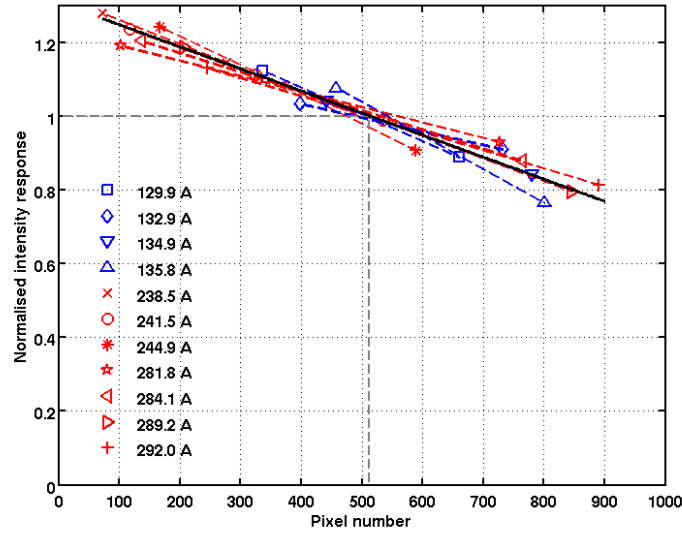
470

471 The synthesis of all these measurements is presented on **Fig. 6**. The results show that
472 the intensity response is a decreasing function of the spectral line position in the direction of
473 increasing pixel number (corresponding to increasing wavelengths) on the MCP detector in
474 the useful range (between pixels 70 and 900 for the LW detector). The measurements show
475 that the response at both ends of the detector (below pixel 70 and above pixel 900) is
476 substantially degraded with respect to the major part of the detector range. This is due to the
477 fact that the size of the PDA is slightly larger than the fiber optics bundle size. One notices
478 that the unuseful portion on the large pixel number extremity is wider than that on the small
479 pixel number extremity. This indicates that the bundle is not perfectly centred on the
480 photodiode array. Both ends of the detector have thus been excluded from the study.

481 A straight line has been fitted to the data and the correction factor curve thus obtained
482 has been normalised so that it is 1 in the middle of the detector (pixel 512 here). The
483 spreading of the points around a given position and wavelength in **Fig. 6** indicates that the
484 measurement fluctuations are dominant over the spatial inhomogeneities along the detector.
485 The response decrease along the detector seems to be mostly related to the varying response
486 of the MCP with the photon incidence angle. Indeed it is known that the MCP quantum
487 efficiency decreases as the incoming photon angle with the grating plane becomes more
488 grazing.

489 In **Fig. 6**, the average slope for the group of lines around 130 Å does not show a
490 significant difference with that for the group in the range 240-292 Å (it would correspond to a
491 response difference of less than 3%). Therefore we can consider that the wavelength
492 dependence of the detector response spatial variation can be neglected. As no data in the short
493 (10-70 Å) wavelength range are available for this calibration campaign, the average decrease
494 of **Fig. 6** was used to correct all the line intensity measurements performed for the Manson
495 source and the branching ratio methods (**Figure 5** includes these corrections.) As the intensity
496 response curve introduces a maximum correction of about 20%, which is small compared
497 with the global uncertainty estimated in Section 4.2, it was not necessary to make this
498 correction for the CRM calibration above 200 Å.

499



500

501 **Figure 6:** Intensity response of the LW detector assembly as a function of the line position on
 502 the detector (measured in pixels). Each symbol represents a different spectral line (see list on
 503 Table 4). Dashed line: final correction factor.

504

505 **6. Summary and conclusion**

506 The grazing incidence spectrometer operated on Tore Supra with a 600g/mm grating
 507 blazed at 1.5° has been absolutely calibrated over most of its wavelength coverage, i. e. 9.9-
 508 312 Å. For the lower part of this domain (9.9-113 Å) we have used an ultrasoft-X ray source
 509 calibrated against a gas flow proportional counter set up with a 100% efficiency. For the rest
 510 of the wavelength domain we have used the branching ratio method for absolute calibration
 511 transfer and collisional-radiative modelling of line intensity ratios for relative calibration.

512 The results show that the spectrometer sensitivity has improved with respect to the
 513 previous setup thanks to the new grating and the double multichannel plates in chevron
 514 configuration. The spectrometer is most sensitive in the 50-200 Å range, with a steep decrease
 515 below 50 Å. On the long wavelength side the sensitivity decrease is not as steep. In fact, after
 516 the present calibration procedure we have exchanged the 600 g/mm grating with a 300 g/mm
 517 one and obtained useful measurements up to 680 Å.

518 The uncertainties have been calculated for each individual calibration wavelength. Due
 519 to the variety of methods used for the whole wavelength range, it is not straightforward to
 520 determine a precise global uncertainty. We estimate a 20% uncertainty below 120 Å, where
 521 direct absolute calibration was obtained with the ultrasoft-X ray source, and 35% in the range
 522 120-180 Å where the line branching ratio method was used. In the range above 180 Å where
 523 only the relative calibration procedure (collisional-radiative modelling of line intensity ratios)

524 was available, the uncertainty is estimated to 50% or even more. This reflects the larger
525 uncertainties and the spreading of the individual calibration points in the LW range.

526

527

528

529 **Bibliography**

530

531 [1] E. Hinnov and W. Hofmann, J. Opt. Soc. Am. 53 (1963) 1259

532 [2] J.L. Schwob and C. Breton, C. R. Acad. Sc. 261 (1965) 1476

533 [3] J.L. Schwob, C. R. Acad. Sc. 262 (1966) 1264

534 [4] J.L. Schwob, CEA report R-3359 (1969)

535 [5] K. Lawson, I. Coffey, J. Zacks, M.F. Stamp and JET-EFDA contributors, J. Instr. 4 (2009)
536 P04013

537 [6] J. Park, G.V. Brown, M.B. Schneider, H.A. Baldis, K.V. Cone, R.L. Kelley, C.A.
538 Kilbourne, E.W. Magee, M.J. May and F.S. Porter, Rev. Sci. Instrum. 81 (2010) 10E319

539 [7] J.L. Schwob, A.W. Wouters, S. Suckewer and M. Finkenthal, Rev. Sci. Instrum. 58 (9)
540 (1987) 1601

541 [8] R. Prakash, J. Jain, V. Kumar, R. Manchanda, B. Agarwal, M.B. Chowduri, S. Banerjee
542 and P. Vasu, J. Phys. B 43 (2010) 144012

543 [9] J.E. Manson, Manson model 5 ultrasoft-X ray calibration source, 1985; Austin Instruments
544 Inc.

545 [10] D. Stutman, S. Kovnovich, M. Finkenthal, A. Zwicker and H.W. Moos, Rev. Sci.
546 Instrum. 62 (1991) 2719

547 [11] C. Breton and J. L. Schwob, C. R. Acad. Sc. 260 (1965) 461

548 [12] H. P. Summers, *Atomic Data and Analysis Structure User Manual*
549 (2007) <http://www.adas.ac.uk/>

550 [13] D. Villegas, R. Guirlet, C. Bourdelle, X. Garbet, G.T. Hoang, R. Sabot, F. Imbeaux and
551 J.L. Ségui, Nucl. Fusion 54 (2014) 073011

552 [14] C. Biedermann, R. Radtke, J.L. Schwob, P. Mandelbaum, R. Doron, T. Fuchs and G.
553 Fussmann, Physica Scripta T92 (2001) 85

554 [15] R. Radtke, C. Biedermann, J.L. Schwob, P. Mandelbaum and R. Doron, Phys. Rev. A 64
555 (2001) 012720